Analytica Chimica Acta 1034 (2018) 137–143

Contents lists available at ScienceDirect

Analytica Chimica Acta

journal homepage: www.elsevier.com/locate/aca

Electrochemical biosensor made with tyrosinase immobilized in a matrix of nanodiamonds and potato starch for detecting phenolic compounds

Jéssica Rocha Camargo [a], Marina Baccarin [b], Paulo A. Raymundo-Pereira [c], Anderson M. Campos [d], Geiser G. Oliveira [b], Orlando Fatibello-Filho [b], Osvaldo N. Oliveira Jr. [c], Bruno C. Janegitz [a, *]

[a] Department of Natural Sciences, Mathematics and Education, Federal University of São Carlos, 13600-970, Araras, SP, Brazil
[b] Department of Chemistry, Federal University of São Carlos, 13565-970, São Carlos, SP, Brazil
[c] São Carlos Institute of Physics, University of São Paulo, CEP 13560–970, São Carlos, SP, Brazil
[d] São Carlos Institute of Chemistry, University of São Paulo, São Carlos, São Paulo CEP 13566-590, Brazil

HIGHLIGHTS

- Biosensor made with a biocompatible thin film containing nanodiamonds and potato starch, coated with tyrosinase.
- The biosensor detected catechol with a low detection limit.
- Catechol could also be detected in tap and river water samples.
- Estimated cost per sensing unit of only US$ 0.04

GRAPHICAL ABSTRACT

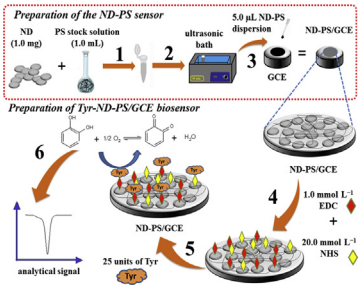

ARTICLE INFO

Article history:
Received 16 January 2018
Received in revised form
30 May 2018
Accepted 1 June 2018
Available online 5 June 2018

Keywords:
Biopolymer
Nanodiamonds
Potato starch
Catechol detection
Biosensing
Tap and river water sample

ABSTRACT

The envisaged ubiquitous sensing and biosensing for varied applications has motivated materials development toward low cost, biocompatible platforms. In this paper, we demonstrate that carbon nanodiamonds (NDs) can be combined with potato starch (PS) and be deposited on a glassy carbon electrode (GCE) in the form of a homogeneous, rough film, with electroanalytical performance tuned by varying the relative ND-PS concentration. As a proof of concept, the ND/PS film served as matrix to immobilize tyrosinase (Tyr) and the resulting Tyr-ND-PS/GCE biosensor was suitable to detect catechol using differential pulse voltammetry with detection limit of 3.9×10^{-7} mol L^{-1} in the range between 5.0×10^{-6} and 7.4×10^{-4} mol L^{-1}. Catechol could also be detected in river and tap water samples. This high sensitivity, competitive with biosensors made with more sophisticated procedures and materials in the literature, is attributed to the large surface area and conductivity imparted by the small NDs (<5 nm). In addition, the ND-PS matrix may have its use extended to immobilize other enzymes and biomolecules, thus representing a potential biocompatible platform for ubiquitous biosensing.

1. Introduction

Sensing and biosensing are bound to become ubiquitous with

* Corresponding author.
E-mail address: brunocj@ufscar.br (B.C. Janegitz).

https://doi.org/10.1016/j.aca.2018.06.001
0003-2670/

the exciting developments in the Big Data movement [1] with the Internet of Things [2], and the prospects of computer-assisted diagnostics systems [3]. Many are the requirements for such ambitious endeavours to be turned into reality as sensors and biosensors may need to be integrated into wearable and/or implantable devices [4]. The large number of methodologies already employed for detection will have to be explored and even adapted or extended, and the same applies to the materials used for making the sensing units. When remote monitoring is desired, for instance, principles of detection based on optical measurements are usually preferred [5]. In other applications such as monitoring water quality and the environment or detecting food contamination or diseases [6], electroanalytical techniques could be preferred. Common to the stringent requirements alluded to is the need of low cost technologies. Analytical tools that require expensive, sophisticated equipment and trained personnel to operate them are not suitable.

Electrochemical sensors that can be made of cheap materials, and be miniaturized into portable devices [7], seem strong candidates for fulfilling the requirements of ubiquitous sensing. It is in this context that our team have tried to exploit carbon-based materials and natural starch from tapioca and potato in matrices for sensors and biosensors [8,9]. In this paper, more specifically, we employ carbon nanodiamonds (NDs) and potato starch to immobilize the enzyme tyrosinase, with which detection of catechol (CAT) is performed with differential pulse voltammetry. The choice of NDs was inspired by the successful use of carbon nanomaterials in biosensing [10–14] owing to their possible high conductivity, mechanical strength, ease with which they are modified, and biocompatibility. In fact, the success in applications of carbon nanotubes and graphene has stirred significant research into other forms of nanostructured carbon, which have been found in many cases equally efficient for applications with the advantage of lower cost of production. Indeed, carbon black, printex carbon, carbon nano-onions and carbon nanodiamonds (NDs) have all been used in electroanalytical applications [13,15,16].

Some of these carbon forms are not new at all. NDs, for instance, were first synthesized in the 1960s [17] with irradiation of graphite by shock waves generated by detonation of a mixture of TNT (2-methyl-1,3,5-trinitrobenzene, $(C_6H_2(NO_2)_3CH_3)$ and RDX (hexogen, $C_3H_6N_6O_6$). After detonation, the remaining soot was filled with ND particles, which were purified via oxidation and/or treatment with mineral acids. In recent years, NDs have been produced with a commercial-scale detonation technique, laser ablation, and plasma-assisted chemical vapour deposition [18]. NDs are made of gray particles smaller than 10 nm within a tetrahedral structure of sp^3 hybridized carbons, delocalized π bonds, and oxygen functional groups on their surfaces [19,20]. These characteristics make NDs versatile [21], e.g. to use as carriers for anticancer drugs [22], in sensors and biosensors [23–26] to detect antibodies [24], glucose [25], hemoglobin [26], and cytochrome *c* [27].

While ND themselves can serve as matrix in a film form for building biosensors [15], synergy may be reached if they are associated with a natural biopolymer such as potato starch. Indeed, we shall show here that the electroanalytical performance can be varied significantly depending on the relative concentration of NDs and potato starch (PS). We chose PS due to its physicochemical stability, simplicity of manipulation, biocompatibility, abundance and low cost. It is formed by two classes of carbohydrates with ca. 20% m/m of amylose and 80% m/m amylopectin [28,29], which confer stability and resistance. PS also has functional groups leading to a high solubility in water when heated [30], thus permitting to obtain stable, homogeneous dispersions.

As a proof-of-principle, we employed the NDs/PS matrix to immobilize tyrosinase with which we detect catechol ($C_6H_4(OH)_2$, CAT), a phenolic compound produced by phenol hydroxylation using H_2O_2. CAT was selected because it has been investigated extensively, including with detection in river water samples [31–38], and therefore we compare the performance of our electrochemical biosensor with a considerable body of literature. CAT is a toxic pollutant originating from pesticides, plastics and from residues from refineries and petrochemical industries. Because such residues containing CAT are sometimes improperly discharged into the environment, there is a potential hazard for human health [39].

2. Experimental

2.1. Materials and methods

NDs (nanopowder, < 10-nm particle size), Tyr 1000 unit/mg (from mushroom), CAT, KCl, $NaNO_3$, $Pb(NO_3)_2$, $CaCl_2.2H_2O$, Na_2SO_4, $SnCl_2$, $K_3[Fe(CN)_6]$, $K_4[Fe(CN)_6]$, acetic acid, 1-ethyl-3-[3-dimethylaminopropyl] carbodiimide (EDC) and N-hydroxysuccinimide (NHS) were acquired from Sigma-Aldrich. PS was purchased at a local supermarket from Yoki® (brand name). Ultrapure water (resistivity > 18.0 MΩ cm) from a Millipore Milli-Q system (Billerica, USA) was used to prepare all solutions. The 0.20 mol L^{-1} phosphate buffer solutions (pH 5.7 to 8.0) were prepared with Na_2HPO_4 and NaH_2PO_4 from Sigma-Aldrich and used as supporting electrolytes.

The morphology of NDs-PS biopolymer films was recorded using scanning electron microscopy coupled with energy-dispersive X-ray spectroscopy (SEM-EDX) with a LEO-440 microscope (Zeiss-Leica), and with transmission electron microscopy (TEM) with a FEI TECNAI G2F20 microscope at an acceleration voltage of 200 kV. The NDs were studied using the Nicolet iS50 Fourier transform-infrared (FT-IR) spectrometer (Thermo Scientific). Differential pulse voltammetry (DPV) and cyclic voltammetry measurements were conducted with an Autolab PGSTAT-30 (Ecochemie) potentiostat/galvanostat, coupled to a microcomputer controlled by 4.9 GPES software. A three-electrode cell was used with a counter electrode (platinum plate), a reference electrode of Ag/AgCl (3.0 mol L^{-1} KCl), and a working electrode (GCE, PS/GCE, NDs-PS/GCE or Tyr-ND-PS/GCE). Electrochemical impedance spectroscopy (EIS) analysis was performed with 5.0×10^{-3} mol L^{-1} $K_3[Fe(CN)_6]/K_4[Fe(CN)_6]$ in a 0.10 mol L^{-1} KCl solution using NOVA software. The frequency ranged from 0.10 to 100 kHz, in an open circuit potential, with an amplitude of 10 mV.

2.2. Preparation of NDs-PS dispersion and biosensor fabrication

Commercial PS (1.0 mg) was dispersed in 5.0% (v/v) acetic acid aqueous solution and left under stirring for 1 h at 85 °C. The resulting suspension was stored under refrigeration. A scheme to fabricate NDs-PS/GCE and Tyr-NDs-PS/GCE sensors is shown in Fig. 1. Step 1 consists in dispersing 1.0 mg of NDs in 1.0 mL of PS solution and then using ultrasonication for 30 min (step 2). 5.0 μL of NDs-PS were dropped on the GCE surface (Ø = 3.0 mm) (step 3), previously cleaned as described in Ref. [40]. The NDs-PS/GCE platform was dried during 12 h at room temperature. Tyrosinase was immobilized covalently using a solution containing 1.0×10^{-3} mol L^{-1} of EDC and 20×10^{-3} mol L^{-1} of NHS for 2 h (step 4) followed by immersion in a solution containing 100 μL of 0.20 mol L^{-1} phosphate buffer (pH 6.6) and 25 units of Tyr (step 5). The Tyr-NDs-PS/GCE biosensor was used to detect CAT in river and tap water samples (step 6).

2.3. Water samples collection and analytical procedures

Tap water samples (or distribution water) were collected in the Araras city (SP – Brazil) with geographical coordinates:

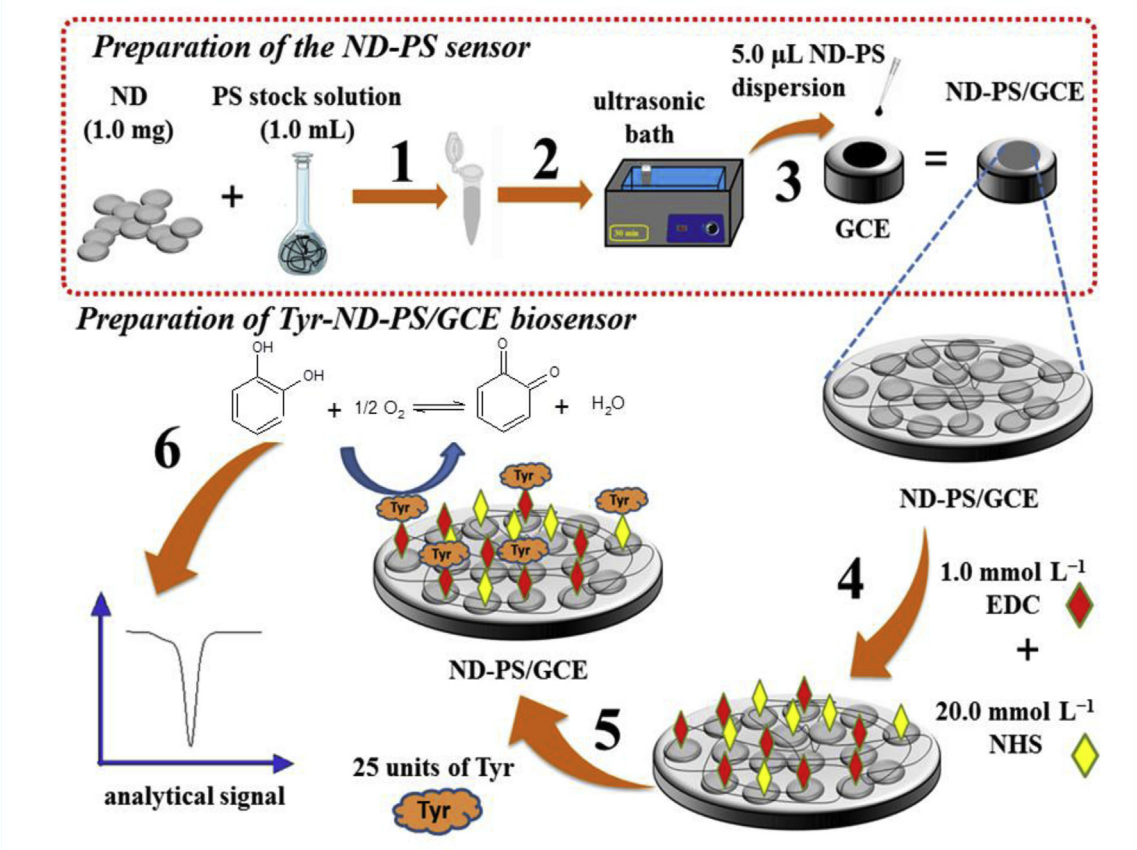

Fig. 1. Scheme of ND-PS/GCE and of Tyr-ND-PS/GCE preparation. Step 1: ND was dispersed in PS solution. Step 2: ND-PS dispersion was ultrasonicated for 30 min. Step 3: 5.0 µL of the ND-PS were dropped on the GCE surface. Step 4: ND-PS/GCE was immersed in a solution containing 1-ethyl-3-[3-dimethylaminopropyl] carbodiimide (EDC) and N-hydroxysuccinimide (NHS) for 2 h. Step 5: ND-PS/GCE was immersed in a solution containing 25 units of Tyr. Step 6: Detection of CAT in samples of tap and river water with the Tyr-ND-PS/GCE biosensor.

22°18′22.6″S 47°22′52.1″O, while the river water samples was taken from the Monjolinho River, located in São Carlos city (SP – Brazil) with geographical coordinates: 21°59′11″S 47°52′55″O. River water samples were filtered through a 3-µm filter paper (Nalgon) for removal of small leaves and suspensions. Tap water was used without any prior treatment. All samples were stirred, homogenized, and fortified with known amounts of CAT. The tap water samples were identified as A (2.4×10^{-4} mol L^{-1} CAT), B (4.7×10^{-4} mol L^{-1} CAT), and C (7.4×10^{-4} mol L^{-1} CAT), while the river water samples were D (2.4×10^{-4} mol L^{-1} CAT), E (4.7×10^{-4} mol L^{-1} CAT), and F (7.4×10^{-4} mol L^{-1} CAT).

The parameters used in the DPV technique were optimized as follows: scan rate 25 mV s^{-1}, amplitude 100 mV, modulation time 30 ms, pH = 6.6. The limit of detection (LOD) was calculated as $3 \times SD/S$, where *SD* is the standard deviation of the 10 background measurements and *S* is the slope of the analytical curve. The repeatability studies were conducted in a solution containing 1.2×10^{-4} mol L^{-1} CAT. Selectivity studies were performed with 9.0×10^{-5} mol L^{-1} CAT solution in the presence of potential interfering substances such as KCl, $NaNO_3$, $Pb(NO_3)_2$, $CaCl_2.2H_2O$, Na_2SO_4, and $SnCl_2$. The biosensor Tyr-NDs-PS/GCE was stored in phosphate buffer solution in a refrigerator at 4 °C during the long-term stability studies.

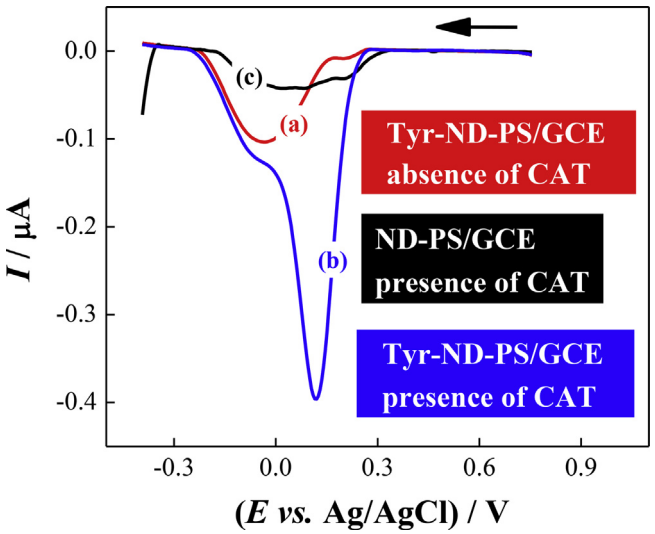

Fig. 2. DP voltammograms in the absence of catechol (CAT) in **(a)** and in the presence of 1.0×10^{-5} mol L^{-1} CAT with Tyr-ND-PS/GCE biosensor in **(b)**. Catechol detection (1.0×10^{-5} mol L^{-1}) at ND-PS/GCE in **(c)**. Measurements were carried out in 0.20 mol L^{-1} phosphate buffer (pH 6.6).

3. Results and discussion

3.1. Electrochemical detection of CAT

Typical differential pulse voltammograms are shown in Fig. 2, where the reduction current (0.1 V vs. Ag/AgCl) recorded with the Tyr-NDs-PS/GCE surface is the highest due to the enzymatic catalysis of Tyr. The mechanism of detection can be described with the tyrosinase enzyme catalysing biological reactions of phenols

hydroxylation and conversion of *o*-diphenols to o-quinone [41]. These catalytic effects should enhance the CAT analytical signal when compared to the non-enzymatic devices [42] as it clear with the comparison in Fig. 2 for NDs-PS/GCE (without enzyme) in **(c)**. The peak near 0 V appeared due to the reduction of Cu^{2+} ions in the active centre of the biomolecule. In addition, the results confirm that the enzyme was efficiently linked onto the NDs-PS biopolymer surface. This may represent a new strategy to immobilize biomolecules, alternative to traditional methodologies using chitosan and dihexadecylphosphate [43].

The cathodic peak current increased linearly in the CAT concentration range between 5.0×10^{-6} and 7.4×10^{-4} mol L^{-1} according to DPV data in Fig. 3. A calibration curve in the inset was obtained from $I\,(\mu A) = -\,5.1 \times 10^{-7} + 0.023\ C_{CAT}\ (\mu mol\ L^{-1})$ with a linear correlation (r) of 0.992 and LOD of 3.9×10^{-6} mol L^{-1}.

Intra-day and inter-day repeatability tests were conducted with five measurements using 1.2×10^{-4} mol L^{-1} CAT solutions. The relative standard deviations (RSD) were 3.7 and 4.0%, respectively. The low percentages suggest a satisfactory precision of the proposed procedure. Possible effects from interferents were checked using solutions with 9.0×10^{-4} mol L^{-1} of CAT to which appropriate amounts of $CaCl_2.2H_2O$, KCl, $NaNO_3$, Na_2SO_4, $Pb(NO_3)_2$ and $SnCl_2$ were added to reach a final concentration of 9.0×10^{-4} mol L^{-1}. The percentages of change in current signals were 0.5, 4.1, 3.6, 8.8, 3.13, 6.9% for $CaCl_2.2H_2O$, KCl, $NaNO_3$, Na_2SO_4, $Pb(NO_3)_2$ and $SnCl_2$, respectively, indicating the selectivity of the method (Fig. S1 in the Supporting Information). The long-term stability of the biosensor was studied using a 1.2×10^{-4} mol L^{-1} CAT solution, and the measured current was constant during 17 days (Fig. S2 in the Supporting Information). Therefore, there is no difficulty with stability for using these sensing units in disposable devices.

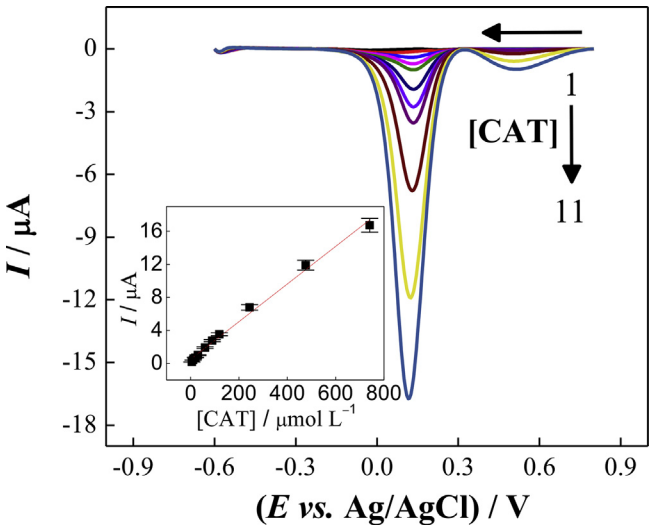

Fig. 3. DP voltammograms for detecting CAT from 5.0×10^{-6} to 7.4×10^{-4} mol L^{-1} in 0.20 mol L^{-1} phosphate buffer (pH 6.6) using Tyr-ND-PS/GCE. The inset shows the analytical curve (n = 3).

The Tyr-NDs-PS/GCE biosensor was used to detect CAT in tap and river water samples (A to C were tap water samples and D to F were river water samples). Each water sample was prepared with different CAT concentrations, measured in three replicates for each sample and the results are shown in Table S1 in the Supporting Information. As can be inferred from the recovery results, which varied from 80 to 118%, the maximum interference from the water sample matrix was 20.0%. This specification is suitable for detecting CAT in the environment.

The performance of the Tyr-NDs-PS/GCE biosensor was compared with other tyrosinase-containing biosensors, with the analytical features listed in Table 1. Tyr-NDs-PS/GCE performed similarly to previous biosensors in terms of linear range and LOD, but was advantageous with regard to easy preparation, fast response and selectivity. Also significant is the non-toxic, low resistivity and environmentally friendly nature of PS.

3.2. Electrochemical features of the NDs-PS/GCE biopolymer

The NDs-PS/GCE sensor had lower ΔEp ($\Delta E_p = E_{pa} - E_{pc}$) and higher current than PS/GCE or GCE, as shown in Fig. 4a. This indicates an increase in conductivity and surface area promoted by synergy between NDs and PS. However, an excess of NDs on the GCE surface leads to a decrease in peak currents as seen in Fig. S3 in which the NDs mass in the NDs-PS biopolymer increased from 1.0 to 3.0 mg. The Nyquist diagrams in Fig. 4b were fitted with a Randle's modified equivalent circuit [R_s (CPE [$R_{ct}Z_W$])], where R_s is the solution resistance, R_{ct} is the charge transfer resistance, *CPE* is a constant phase element and Z_W is the Warburg impedance. R_{ct} in ascending order was NDs-PS/GCE (163.4 Ω) < PS/GCE (318.8 Ω) < GCE (716.2 Ω), which confirms the faster electron transfer for NDs-PS/GCE in comparison to bare GCE and PS/GCE.

Fig. 4c and d shows cyclic voltammograms at scan rates from 50 to 350 mV s^{-1} with the corresponding I_a (anodic peak current) *vs.* $v^{1/2}$ (square root of scan rate) curves shown in the insets. With the Randles-Sevcik equation: $I_a = 2.69 \times 10^5\ A\ C\ D^{1/2}\ n^{3/2}\ v^{1/2}$ where I_a is the anodic peak current (A), A is the electroactive area (cm^2), C is the concentration of $[Fe(CN)_6]^{3-}$ solution (mol cm^{-3}), D (7.6×10^{-6} cm^2 s^{-1}) [44] is the diffusion coefficient of the molecule in solution (cm^2 s^{-1}), n is the number of electrons involved in the redox reaction and v is the potential scan rate (V s^{-1}). The estimated electroactive area was 0.10 and 0.080 cm^2 for NDs-PS/GCE and GCE, respectively, suggesting an increase of 25%.

3.3. Morphology of NDs-PS/GCE

A homogeneous, rough biopolymer film is seen on the SEM

Table 1
Comparison between Tyr-ND-PS/GCE and tyrosinase-containing biosensors for CAT quantification.

Sensor	Linear range (mol L^{-1})	LOD (mol L^{-1})	Ref.
PEDOT-rGO-Fe_2O_3-PPO/GCE[a]	4.0×10^{-8} to 6.2×10^{-5}	7.0×10^{-9}	[33]
Tyr-MWNTs-PDDA/GCE[b]	2.0×10^{-6} to 1.0×10^{-4}	6.6×10^{-7}	[35]
MWNT-Nafion-Tyr/GCE	1.0×10^{-6} to 1.9×10^{-5}	1.3×10^{-7}	[36]
Tyr/ZnO/GCE	1.0×10^{-5} to 4.0×10^{-2}	6.0×10^{-6}	[37]
Tyr-PO4—PPy/Pt[c]	1.0×10^{-5} to 1.2×10^{-4}	8.4×10^{-7}	[38]
Tyr-ND-PS/GCE	5.0×10^{-6} to 7.4×10^{-4}	3.9×10^{-7}	This work

[a] PEDOT-rGO-Fe_2O_3-PPO/GCE = poly (3,4-ethylenedioxythiophene) - reduced graphene oxide - Fe_2O_3 nanoparticles - polyphenol oxidase/glassy carbon electrode.
[b] Tyr-MWNTs-PDDA/GCE = tyrosinase - multi-walled carbon nanotubes - polydiallyldimethylammonium chloride/glassy carbon electrode.
[c] Tyr-PO_4-PPy/Pt = Tyr - PO_4 — polypyrrole/platinum electrode.

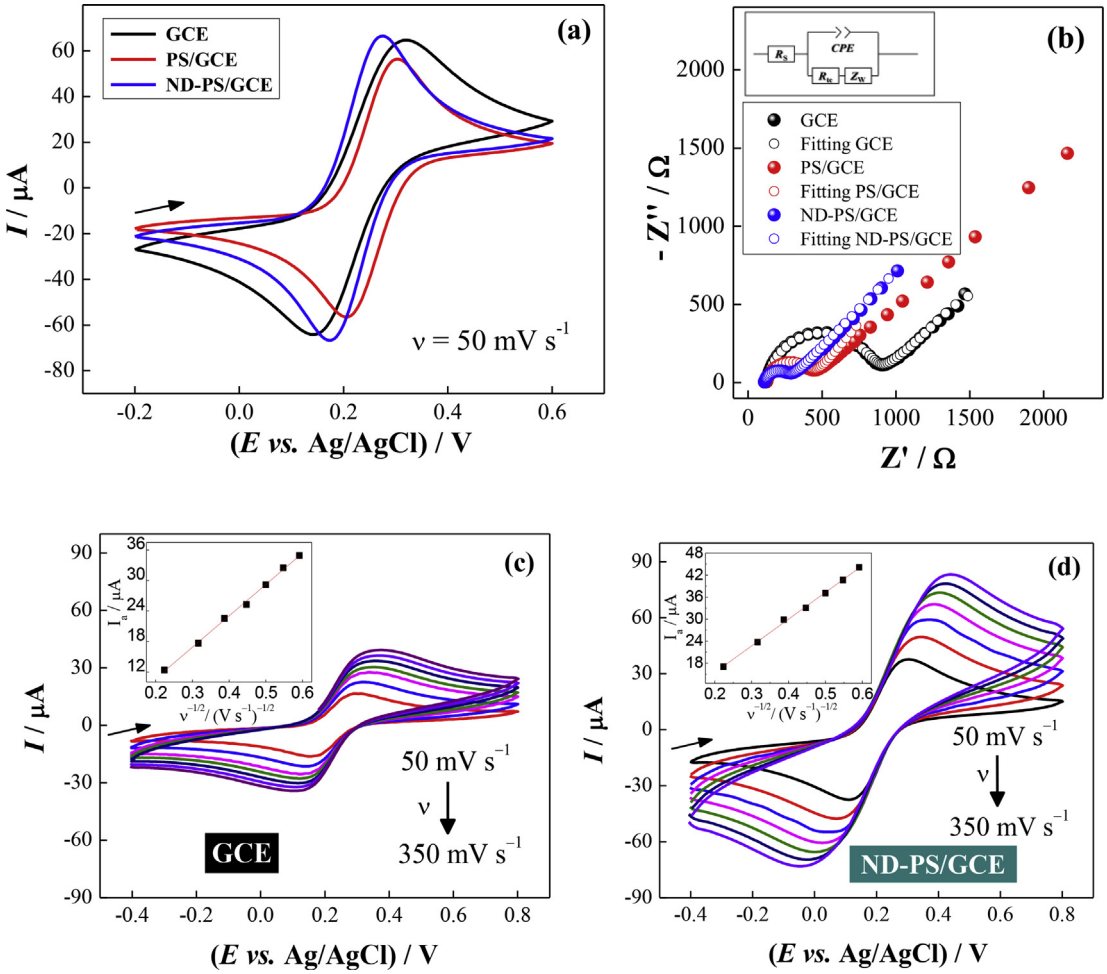

Fig. 4. (a) Cyclic voltammograms for 1.0×10^{-5} mol L^{-1} $[Fe(CN)_6]^{3-}$ with GCE, PS/GCE and ND-PS/GCE, scan rate of 50 mV s^{-1}. (b) Nyquist diagrams for GCE, PS/GCE, and ND-PS/GCE for 5.0×10^{-3} mol L^{-1} $[Fe(CN)_6]^{4-/3-}$. (c) Cyclic voltammograms for 1.0×10^{-5} mol L^{-1} $[Fe(CN)_6]^{3-}$ with GCE and (d) ND-PS/GCE at scan rates from 50 to 350 mV s^{-1}. The insets show I_a *vs.* $\nu^{1/2}$ curves. All experiments were performed in 0.10 mol L^{-1} KCl solution.

micrograph in Fig. 5a while Fig. 5b highlights the agglomeration of NDs in PS. According to the TEM micrographs in Fig. 5c and d, NDs are spherical with diameter smaller than 5 nm, being uniformly distributed on the PS biopolymer. The EDX spectrum in Fig. 5e shows copper from the grids, in addition to carbon and oxygen from NDs-PS biopolymer, thus indicating the absence of contaminants. The corresponding electron diffraction (SAED) pattern (*inset* in Fig. 5e) confirmed the absence of crystallinity in NDs structure. The FTIR spectrum in Fig. 5f shows the graphitic nature of the carbon, the hetero-nuclear functional group vibrations and polar bonds with a strong, broad adsorption at 3412 cm^{-1} assigned to O–H stretching. The band at 1730 cm^{-1} is assigned to C=O stretching of COOH groups, while those at 1622 and 1130 cm^{-1} can be associated with absorption of ketone groups (C=O) [45]. Bands at 2925, 2851 and 1340 cm^{-1} are assigned to the bending modes of CH_3, CH_2 and C=C [27,46]. This last one indicates π bonds at the ND surface, which is one of the groups responsible for the material conductivity. The size, uniform distribution and chemical surface of NDs are useful for sensors due to the increase in conductivity and surface area leading to higher electroanalytical signals desired in (bio)sensing devices.

4. Conclusion

A potential biocompatible matrix made of NDs and PS was employed to immobilize tyrosinase with which CAT was detected in tap and river water samples. A low LOD of 3.9×10^{-6} mol L^{-1} was achieved using the DPV technique due to the large surface area and conductivity promoted by NDs when they were added at an optimized relative concentration. The Tyr-NDs-PS/GCE biosensor exhibited an analytical performance similar to previously reported biosensors with the advantages of easy preparation, fast response, selectivity and relative low cost.

Taken together the results presented here amount to a demonstration that the non-toxic, environmentally friendly PS biopolymer may be combined with NDs and have their surface properties tuned by varying their relative concentrations in order to optimize electroanalytical performance. The immobilization of tyrosinase was just performed as a proof-of-principle experiment, for NDs/PS can be used as matrix for many other enzymes and biomolecules. The possible biocompatibility of the matrix may be valuable for the needed ubiquitous sensing in IoT and other applications.

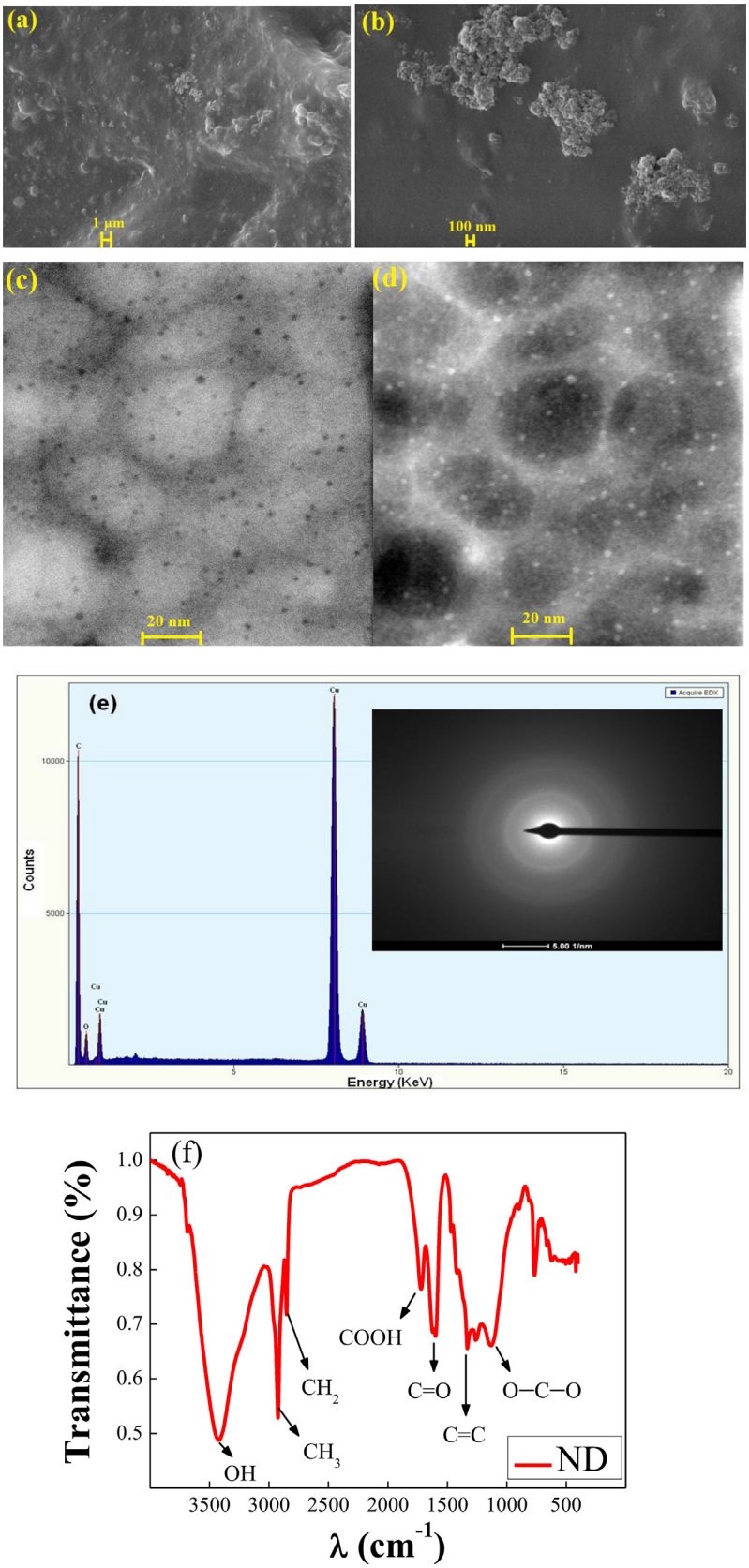

Fig. 5. SEM micrographs of ND-PS biopolymer at a magnification of 10,000x (a) and 50,000x (b). TEM micrographs of ND-PS biopolymer in bright field (c) and in dark field (d). Corresponding EDX spectrum of ND-PS and electron diffraction (SAED) pattern of a selected area (inset) (e). FTIR spectrum of ND powder (f).

Acknowledgments

The authors acknowledge financial support from the Brazilian funding agencies FAPESP (2015/19099-2, 2013/14262-7 and 2016/01919-6), CNPq (444150/2014-5), and CAPES. The authors are also grateful to Marcio de Paula and CAQI/IQSC/USP for the use of SEM facilities, and to the Structural Characterization Laboratory/Department of Materials Engineering of the Federal University of São Carlos (LCE/DEMa/UFSCar) for technical support during TEM analyses.

Appendix A. Supplementary data

Supplementary data related to this article can be found at https://doi.org/10.1016/j.aca.2018.06.001.

References

[1] J. Andreu-Perez, C.C.Y. Poon, R.D. Merrifield, S.T.C. Wong, G.Z. Yang, Big data for health, Ieee J Biomed Health 19 (2015) 1193–1208.
[2] H. Gupta, A.V. Dastjerdi, S.K. Ghosh, R. Buyya, iFogSim: a toolkit for modeling and simulation of resource management techniques in the Internet of Things, Edge and Fog computing environments, Software Pract. Ex. 47 (2017) 1275–1296.
[3] J.F. Rodrigues, F.V. Paulovich, M.C.F. de Oliveira, O.N. Oliveira Jr., On the convergence of nanotechnology and Big Data analysis for computer-aided diagnosis, Nanomedicine 11 (2016) 959–982.
[4] A. Darwish, A.E. Hassanien, Wearable and implantable wireless sensor network solutions for healthcare monitoring, Sensors-Basel 11 (2011) 5561–5595.
[5] C.L. de Camargo, M.B.R. Vicentini, A.L. Gobbi, D.S.T. Martinez, R.S. Lima, Smartphone for point-of-care quantification of protein by bradford assay, J. Braz. Chem. Soc. 28 (2017) 689–693.
[6] S. Cinti, Polymeric materials for printed-based electroanalytical (Bio)Applications, Chemosensors 5 (2017).
[7] S. Cinti, F. Santella, D. Moscone, F. Arduini, Hg2+ detection using a disposable and miniaturized screen-printed electrode modified with nanocomposite carbon black and gold nanoparticles, Environ. Sci. Pollut. Res. 23 (2016) 8192–8199.
[8] G.C.M. de Oliveira, E.P. de Palma, M.H. Kunita, R.A. Medeiros, R. de Matos, K.R. Francisco, B.C. Janegitz, Tapioca biofilm containing nitrogen-doped titanium dioxide nanoparticles for electrochemical detection of 17-beta estradiol, Electroanalysis 29 (2017) 2638–2645.
[9] L.V. Jodar, F.A. Santos, V. Zucolotto, B.C. Janegitz, Electrochemical sensor for estriol hormone detection in biological and environmental samples, J. Solid State Electrochem. 22 (2018) 1431–1438.
[10] B.C. Janegitz, T.A. Silva, A. Wong, L. Ribovski, F.C. Vicentini, M.d.P.T. Sotomayor, O. Fatibello-Filho, The application of graphene for in vitro and in vivo electrochemical biosensing, Biosens. Bioelectron. 89 (2017) 224–233.
[11] M. Mazloum-Ardakani, A. Khoshroo, High performance electrochemical sensor based on fullerene-functionalized carbon nanotubes/ionic liquid: determination of some catecholamines, Electrochem. Commun. 42 (2014) 9–12.
[12] B.S. Sherigara, W. Kutner, F. D'Souza, Electrocatalytic properties and sensor applications of fullerenes and carbon nanotubes, Electroanalysis 15 (2003) 753–772.
[13] T.A. Silva, F.C. Moraes, B.C. Janegitz, O. Fatibello-Filho, Electrochemical biosensors based on nanostructured carbon black: a review, J. Nanomater. 2017 (2017).
[14] J. Wang, Carbon-nanotube based electrochemical biosensors: a review, Electroanalysis 17 (2005) 7–14.
[15] A. Krueger, New carbon materials: biological applications of functionalized nanodiamond materials, Chem. Eur J. 14 (2008) 1382–1390.
[16] O. Mykhailiv, H. Zubyk, M.E. Plonska-Brzezinska, Carbon nano-onions: unique carbon nanostructures with fascinating properties and their potential applications, Inorg. Chim. Acta. 468 (2017) 49–66.
[17] A. Krueger, Diamond nanoparticles: jewels for chemistry and physics, Adv. Mater. 20 (2008) 2445–2449.
[18] V.N. Mochalin, O. Shenderova, D. Ho, Y. Gogotsi, The properties and applications of nanodiamonds, Nat. Nanotechnol. 7 (2012) 11–23.
[19] K.B. Holt, C. Ziegler, D.J. Caruana, J. Zang, E.J. Millán-Barrios, J. Hu, J.S. Foord, Redox properties of undoped 5 nm diamond nanoparticles, Phys. Chem. Chem. Phys. 10 (2008) 303–310.
[20] I. Kulakova, Surface chemistry of nanodiamonds, Phys. Solid State 46 (2004) 636–643.
[21] O.A. Williams, T. Zimmermann, M. Kubovic, A. Denisenko, E. Kohn, R. Jackman, D. Gruen, Electronic properties and applications of ultrananocrystalline diamond, in: Synthesis, Properties and Applications of Ultrananocrystalline Diamond, Springer, 2005, pp. 373–382.
[22] G. Xi, E. Robinson, B. Mania-Farnell, E.F. Vanin, K.-W. Shim, T. Takao, E.V. Allender, C.S. Mayanil, M.B. Soares, D. Ho, Convection-enhanced delivery of nanodiamond drug delivery platforms for intracranial tumor treatment, Nanomedicine 10 (2014) 381–391.
[23] N.B. Simioni, G.G. Oliveira, F.C. Vicentini, M.R. Lanza, B.C. Janegitz, O. Fatibello-Filho, Nanodiamonds stabilized in dihexadecyl phosphate film for electrochemical study and quantification of codeine in biological and pharmaceutical samples, Diam. Relat. Mater. 74 (2017) 191–196.
[24] W. Zhang, K. Patel, A. Schexnider, S. Banu, A.D. Radadia, Nanostructuring of biosensing electrodes with nanodiamonds for antibody immobilization, ACS Nano 8 (2014) 1419–1428.
[25] W. Zhao, J.-J. Xu, Q.-Q. Qiu, H.-Y. Chen, Nanocrystalline diamond modified gold electrode for glucose biosensing, Biosens. Bioelectron. 22 (2006) 649–655.
[26] J.-T. Zhu, C.-G. Shi, J.-J. Xu, H.-Y. Chen, Direct electrochemistry and electrocatalysis of hemoglobin on undoped nanocrystalline diamond modified glassy carbon electrode, Bioelectrochemistry 71 (2007) 243–248.
[27] L.-C.L. Huang, H.-C. Chang, Adsorption and immobilization of cytochrome c on nanodiamonds, Langmuir 20 (2004) 5879–5884.
[28] W.A.d. Silva, J. Pereira, C.W.P.d Carvalho, F.Q. Ferrua, Determination of color, topographic superficial image and contact angle of the biofilms of different starch sources, Cienc. E Agrotecnol 31 (2007) 154–163.
[29] R. Geddes, C. Greenwood, S. Mackenzie, Studies on the biosynthesis of starch granules: Part III. The properties of the components of starches from the growing potato tuber, Carbohydr. Res. 1 (1965) 71–82.
[30] H. Grommers, D. Van Der Krogt, Potato Starch: Production, Modifications and Uses, Starch: Chemistry and Technology, Elsevier Inc, 2009, p. 511.
[31] F. Hu, S. Chen, C. Wang, R. Yuan, D. Yuan, C. Wang, Study on the application of reduced graphene oxide and multiwall carbon nanotubes hybrid materials for simultaneous determination of catechol, hydroquinone, p-cresol and nitrite, Anal. Chim. Acta 724 (2012) 40–46.
[32] F.C. Vicentini, L.L. Garcia, L.C. Figueiredo-Filho, B.C. Janegitz, O. Fatibello-Filho, A biosensor based on gold nanoparticles, dihexadecylphosphate, and tyrosinase for the determination of catechol in natural water, Enzym. Microb. Technol. 84 (2016) 17–23.
[33] V. Sethuraman, P. Muthuraja, J.A. Raj, P. Manisankar, A highly sensitive electrochemical biosensor for catechol using conducting polymer reduced graphene oxide–metal oxide enzyme modified electrode, Biosens. Bioelectron. 84 (2016) 112–119.
[34] G.H. Ribeiro, L.M. Vilarinho, T.d.S. Ramos, A.L. Bogado, L.R. Dinelli, Electrochemical behavior of hydroquinone and catechol at glassy carbon electrode modified by electropolymerization of tetraruthenated oxovanadium porphyrin, Electrochim. Acta 176 (2015) 394–401.
[35] L. Kong, S. Huang, Z. Yue, B. Peng, M. Li, J. Zhang, Sensitive mediator-free tyrosinase biosensor for the determination of 2, 4-dichlorophenol, Microchim. Acta 165 (2009) 203–209.
[36] Y.-C. Tsai, C.-C. Chiu, Amperometric biosensors based on multiwalled carbon nanotube-Nafion-tyrosinase nanobiocomposites for the determination of phenolic compounds, Sens. Actuators, B 125 (2007) 10–16.
[37] L. Chen, B. Gu, G. Zhu, Y. Wu, S. Liu, C. Xu, Electron transfer properties and electrocatalytic behavior of tyrosinase on ZnO nanorod, J. Electroanal. Chem. 617 (2008) 7–13.
[38] C. Apetrei, M. Rodríguez-Méndez, J. De Saja, Amperometric tyrosinase based biosensor using an electropolymerized phosphate-doped polypyrrole film as an immobilization support. Application for detection of phenolic compounds, Electrochim. Acta 56 (2011) 8919–8925.
[39] S.S. Rosatto, R.S. Freire, N. Durán, L.T. Kubota, Biossensores amperométricos para determinação de compostos fenólicos em amostras de interesse ambiental, Quim. Nova 24 (2001) 77–86.
[40] P.A. Raymundo-Pereira, A.M. Campos, C.D. Mendonca, M.L. Calegaro, S.A.S. Machado, O.N. Oliveira, Printex 6L carbon nanoballs used in electrochemical sensors for simultaneous detection of emerging pollutants hydroquinone and paracetamol, Sensor. Actuator. B Chem. 252 (2017) 165–174.
[41] J.C. García-Borrón, F. Solano, Molecular anatomy of tyrosinase and its related proteins: beyond the histidine-bound metal catalytic center, Pigm. Cell Melanoma Res. 15 (2002) 162–173.
[42] V.C. Sanz, M.L. Mena, A. González-Cortés, P. Yanez-Sedeno, J. Pingarrón, Development of a tyrosinase biosensor based on gold nanoparticles-modified glassy carbon electrodes: application to the measurement of a bioelectrochemical polyphenols index in wines, Anal. Chim. Acta 528 (2005) 1–8.
[43] B.C. Janegitz, M. Baccarin, P.A. Raymundo-Pereira, F.A. dos Santos, G.G. Oliveira, S.A.S. Machado, M.R.V. Lanza, O. Fatibello-Filho, V. Zucolotto, The use of dihexadecylphosphate in sensing and biosensing, Sensor. Actuator. B Chem. 220 (2015) 805–813.
[44] A.J. Bard, L.R. Faulkner, Electrochemical Methods: Fundamentals and Applications, Wiley New York, 1980.
[45] O.A. Williams, J. Hees, C. Dieker, W. Jäger, L. Kirste, C.E. Nebel, Size-dependent reactivity of diamond nanoparticles, ACS Nano 4 (2010) 4824–4830.
[46] P.-H. Chung, E. Perevedentseva, J.-S. Tu, C. Chang, C.-L. Cheng, Spectroscopic study of bio-functionalized nanodiamonds, Diam. Relat. Mater. 15 (2006) 622–625.